MEMBRANES

A two-phase model that unifies and extends the classical models of membrane transport

Varun H. Hegde, Michael F. Doherty, Todd M. Squires*

Two models describe solvent transport through swollen, nonporous membranes. The pore-flow model, based on fluid mechanics, works for porous membranes, whereas the solution-diffusion model invokes molecular diffusion to treat nonporous membranes. Both approaches make valid arguments for swollen polymer membranes, but they disagree in their predictions of intramembrane pressure and concentration profiles. Using a fluid-solid model that treats the solvent and membrane matrix as separate phases, we show both classical models to be valid, to represent complementary approaches to the same phenomenon, and to make identical predictions. The fluid-solid model clarifies recent reverse osmosis measurements; provides a predictive and mechanistic basis for empirical high-pressure limiting flux phenomena, in quantitative agreement with classic measurements; and gives a framework to treat nonporous but mechanically heterogeneous membrane materials.

Polymer membranes play an essential role in both classic and emerging technologies, including water treatment, gas separations, fuel cells, and flow batteries (*1*, *2*). Membranes generally fall into two broad classes, on the basis of morphological structure and mechanism of action. Porous membranes (e.g., Fig. 1, A to C) are permeated by fixed pores that permit the passage of some species but not others, typically by means of size exclusion and/or electrostatics (*3*). Examples include the micro-, nano-, and ultrafiltration of contaminated water (*3*). By contrast, nonporous membranes (e.g., Fig. 1D) are structurally homogeneous, with permeability and selectivity determined by solubility and diffusivity within the membrane. Examples include gas separation membranes (*3*), organic solvent nanofiltration (*4*, *5*), and reverse osmosis desalination (*6*).

Two types of models are used to describe transport through these two classes of membranes. Porous membranes are treated using pore-flow (PF) models, in which pressure gradients force fluid to flow within the membrane pores. Nonporous membranes are described using solution-diffusion (SD) models, wherein solute and solvent dissolve into the membrane and diffuse down concentration gradients. Each approach is built on a distinct transport mechanism: PF involves the mechanical forcing of fluid through porous membranes by means of a momentum balance, whereas SD describes the thermodynamic forcing down concentration gradients, as described by a mass balance (*3*).

However, some membranes exhibit features common to both SD and PF mechanisms. Swollen polymer membranes consist of statistically homogeneous polymer meshes, in persistent diffusive motion relative to the permeating fluid, consistent with the SD mechanism (*7*–*9*). At the same time, solvent within the permeating fluid networks may traverse such membranes without ever encountering polymer, and so it would be described by fluid dynamics, consistent with the PF model (*10*–*12*). Decades ago, a spirited debate emerged over which approach is appropriate for swollen membranes (*7*–*12*), which persists to this day. Variants of both models continue to be discussed and criticized, for example, in treating reverse osmosis membranes (*13*, *14*), with ongoing reframing of the classical models (*15*, *16*). For example, recent neutron scattering studies of water transport in polyamide reverse osmosis (PARO) membranes suggested SD to be invalid and motivated a proposed change in the strategic design of future PARO membranes, toward reducing tortuosity rather than enhancing selective solubility and diffusivity (*17*).

Here, we introduce a two-phase fluid-solid (FS) model for solvent transport through swollen, homogeneous membranes that reconciles the PF and SD mechanisms, revealing them to be entirely consistent with one another, meaning that they make quantitatively identical predictions. Moreover, the FS model predicts the PF and SD parameters to be connected through the longitudinal osmotic modulus of the membrane, which can be independently measured. In fact, FS model predictions are consistent with neutron scattering measurements of PARO membranes (*17*), indicating that neither PF nor SD is inappropriate for these membranes.

Background

The PF model treats solvent flux through a membrane as a pressure-driven flow through a porous network with fixed geometry. In principle, the Navier-Stokes equations could be solved to relate the solvent flux to the pressure gradient, if the particular morphology of the membrane were known (*1*) (e.g., isoporous or track-etched membranes in Fig. 1, A and B). More often, however, the pore-scale structure is known, at best, only statistically (e.g., Fig. 1C), instead requiring a Darcy-flow approach, $v_s = -\nabla p/\xi$, wherein a local pressure gradient ∇p drives a local solvent velocity v_s, where ξ is a local solvent/matrix friction coefficient. Because solvent only occupies a volume fraction ϕ_s within the membrane, the volumetric solvent flux J_s is a factor ϕ_s smaller than v_s. The macroscopic solvent flux through a membrane of thickness L is then given by

$$J_s = \frac{\phi_s}{\xi}\frac{\Delta p}{L} \equiv \kappa_{PF}\frac{\Delta p}{L} \quad (1)$$

In practice, the friction coefficient ξ or permeability κ_{PF} is not determined independently but rather is typically extracted from macroscopic permeance measurements. Explicit hydrodynamic calculations for simplified geometries [see the supplementary materials (SM)] relate ξ to pore size R_p and solvent viscosity η, typically via $\xi \sim \eta/R_p^2$ (*18*, *19*).

The SD model describes solvent transport through nonporous membranes, whose uniform structure and composition lack clear, continuous pores. This model assumes solvent to diffuse down concentration gradients within the matrix, with flux

$$J_s = \frac{D}{1-\phi_s}\frac{\Delta\phi_s}{L} \quad (2)$$

where D is the binary diffusivity between solvent and polymer, and $\Delta\phi_s$ is the drop in solvent volume fraction between the feed and permeate sides of the membrane (see the SM). Equation 2 is difficult to apply directly, because the solvent volume fraction profile ϕ_s is generally not known within the membrane. Instead, $\Delta\phi_s$ is related to the transmembrane pressure drop Δp. Imposing contact equilibrium for solvent molecules at the feed and permeate boundaries of the membrane (described in the SM) gives

$$J_s = \kappa_{SD}\frac{\Delta p}{L} \equiv \frac{D\phi_s^0}{1-\phi_s^0}\left(\frac{\overline{V}_s}{RT}\frac{\partial \ln\phi_s}{\partial \ln a_s}\bigg|_{\phi=\phi_0}\right)\frac{\Delta p}{L} \quad (3)$$

where $\overline{V}_s$ and a_s are the molar volume and activity of the solvent, respectively (*2*, *8*).

Both SD and PF approaches have been used to treat solvent transport through highly swollen membranes, and reasonable arguments can be made to support either. The fundamentally diffusive nature of even equilibrium swollen membranes, along with the lack of any clear pores, suggests the stochastic, diffusive approach of SD. However, polymer-free "tubes" of solvent permeate highly swollen membranes,

Department of Chemical Engineering, University of California, Santa Barbara, CA, USA.
*Corresponding author. Email: tsquires@ucsb.edu

along which the hydrodynamic pressure must decrease continually as fluid traverses the membrane—no other element enters the momentum balance within the tube. From this standpoint, the pressure-driven PF approach is warranted.

Both SD and PF models predict flux relations of the same macroscopic form, $J_s = \kappa\Delta p/L$, allowing experimentally measured permeabilities (κ) to be interpreted through either model to determine R_p and ξ for PF, and D and ϕ_s for SD. Without independent measurements of those quantities, macroscopic permeability measurements cannot differentiate between the predictions of the two approaches. Support for SD came from the classic experiments of Rosenbaum and Cotton (*20*), which measured concentration gradients across a multilayer stack of swollen gel membranes. Additionally, Ham and colleagues (*21*) demonstrated that the solvent concentration ϕ_s^0 at the feed-side boundary remains constant as pressure increases. Likewise, Gehman (*22*) measured ϕ_s to decrease on the permeate side, as the membrane was compressed against the support layer. A number of apparent discrepancies arise between the PF and SD treatments of swollen membranes. First, the internal pressure and concentration profiles predicted by these two models appear to be at odds with one another (Fig. 2, C and D). SD predicts the pressure p to be constant within the membrane but a steady gradient in solvent concentration ϕ_s (Fig. 2D). By contrast, PF predicts a pressure gradient ∇p within the membrane but a constant concentration ϕ_s (Fig. 2C). Second, the two models describe solvent transport through fundamentally distinct physical mechanisms. The PF approach is mechanical and deterministic in nature and assumes purely convective flow, whereas SD is stochastic and thermodynamic, driven by mutual diffusion between polymer and solvent. Because the binary diffusive flux adds to the volume-averaged reference velocity in Eq. 2, SD transport contains both diffusive and convective components. However, the Fick's law basis of SD underscores the fundamental role of diffusion. Finally, the flux relations predicted by the SD and PF models depend on physically different, and seemingly unrelated, parameters.

The fluid-solid model for gel dynamics

We now describe the FS model, building on the poroelastic theory developed by Biot and Willis to describe soil compaction (*23*–*25*) and extended to gel dynamics by Tanaka and others (*26*–*29*). This approach has been used to probe gel swelling and deswelling, drying, crack propagation, and water permeation (*29*–*31*) and the dynamic swelling, buckling, wrinkling and folding of thin polymer gel films (*32*). The FS model treats the solvent and polymer matrix individually, as distinct

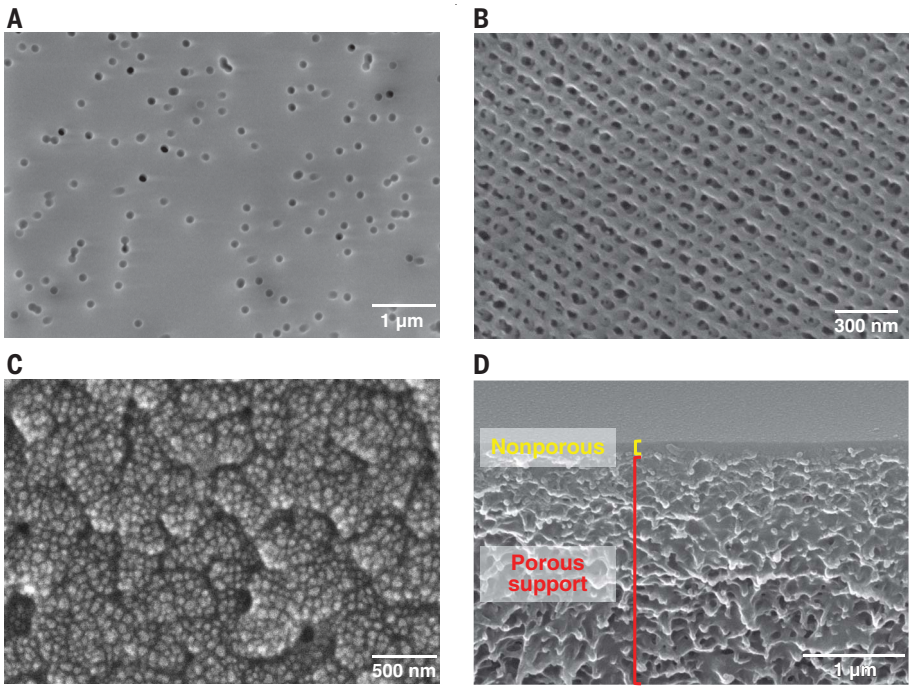

Fig. 1. SEM images of membrane surfaces. (**A**) Scanning electron microscopy (SEM) image of a track-etched polycarbonate membrane with 0.1-μm pores. (**B**) SEM image of an isoporous PS-P4VP [polystyrene-poly(4-vinylpyridine)] membrane where the skin layer is composed of uniformly spaced nanoscale nodules. (**C**) SEM image of a commercial polystyrene-20 ultrafiltration membrane where the skin layer is composed of randomly spaced nanoscale nodules. (**D**) SEM image of a P1-8 asymmetric gas separation membrane with a dense nonporous skin layer bound to a porous support.

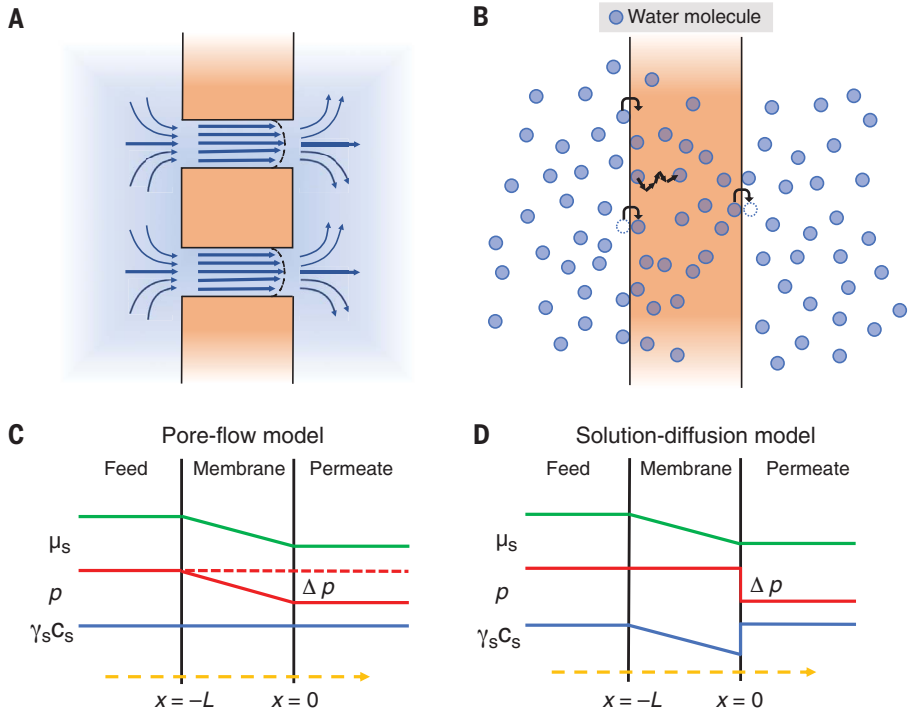

Fig. 2. Classical membrane transport models. (**A** and **B**) Pictorial representation of the pore-flow and solution-diffusion models, respectively. (**C** and **D**) Solvent chemical potential μ_s, pressure p, and solvent activity a_s profiles across a pore-flow and a solution-diffusion membrane, respectively.

IMAGES: MOSTAFA NASSER (FIG. 1A); ALEXANDER BRIDGE (FIG. 1, B TO D)

but interpenetrating phases. The solvent phase is a Newtonian liquid with local velocity field $\mathbf{v}_s(r,t)$ and pressure p and occupies volume fraction ϕ_s. The polymer phase, which occupies volume fraction ϕ_p, is treated as a homogeneous elastic network with displacement field $\mathbf{u}_p(r,t)$ that describes local deformations from the equilibrium state. Together, the solvent and matrix phases fill space—meaning $\phi_s + \phi_p = 1$. Even though the physical solvent and matrix materials are themselves assumed to be incompressible, the matrix network may itself be compressed or dilated, because solvent flows into or out of the network to satisfy the space-filling requirement. The volumetric flux of the FS composite is given by the local volume-averaged velocity, $\mathbf{v} = \phi_p\mathbf{v}_p + \phi_s\mathbf{v}_s$, where $\dot{\mathbf{u}}_p = \partial\mathbf{u}_p/\partial t$ is the local polymer velocity field (*33*).

The governing equations of the FS model

$$\nabla\cdot\mathbf{v} = \nabla\cdot\left[\phi_p\mathbf{u}_p + (1-\phi_p)\mathbf{v}_s\right] = 0 \quad (4)$$

$$\nabla\cdot\boldsymbol{\sigma}_p = \left(K + \frac{G}{3}\right)\nabla(\nabla\cdot\mathbf{u}_p) + G\nabla^2\mathbf{u}_p = -\xi(\mathbf{v}_s - \dot{\mathbf{u}}_p) \quad (5)$$

$$\nabla\cdot\boldsymbol{\sigma}_s = -\nabla p = \xi(\mathbf{v}_s - \dot{\mathbf{u}}_p) \quad (6)$$

enforce conservation of volume, polymer momentum, and solvent momentum, respectively. Polymer and fluid inertia are neglected in both Eq. 5 and Eq. 6, owing to the small length and long time scales of membrane permeation.

The first two terms in the polymer momentum balance (Eq. 5) represent the elastic forces exerted by a deformed, isotropic elastic solid with shear and compressive moduli G and K, respectively (*34*). In the gel context, K is called the osmotic modulus, rather than the bulk modulus, because it is the swollen network that is compressed, rather than the polymer itself, with solvent flowing in or out as needed to conserve volume. The final term represents the drag force (per unit volume) exerted on the network by the solvent, with friction coefficient ξ. The network exerts an equal and opposite force on the fluid phase, which is treated as Darcy flow driven by a hydrodynamic pressure p.

Two important relations emerge from the FS model that play a key role in the PF–SD bridge. The first relates the mutual diffusivity D to the Darcy friction coefficient ξ, and the second relates the thermodynamic properties of a swollen membrane to its mechanical properties.

Solving the polymer momentum equation (Eq. 5) for v_s, inserting into Eq. 4, and relating $\nabla\cdot u_p$ to changes in ϕ_p gives a diffusion-like equation for compressive deformations of the swollen gel

$$\frac{\partial\phi_p}{\partial t} = \frac{M\phi_s}{\xi}\nabla^2\phi_p \quad (7)$$

where $M = K + 4G/3$ is the longitudinal osmotic modulus, associated with free-draining uniaxial compression. Concentration fluctuations of polymer and solvent diffuse relative to one another with mutual diffusivity

$$D = \frac{M\phi_s}{\xi} \equiv M\kappa_{PF} \quad (8)$$

which is called the collective diffusivity by the gel dynamics community (*27*–*29*, *35*). The relationship between the collective diffusivity, which follows from deterministic arguments, and the stochastic solvent-polymer mutual diffusivity, is a consequence of the fluctuation-dissipation theorem, analogous to the Stokes-Einstein relation. Indeed, Paul and Ebra-Lima suggested a relation of this sort should exist (*5*).

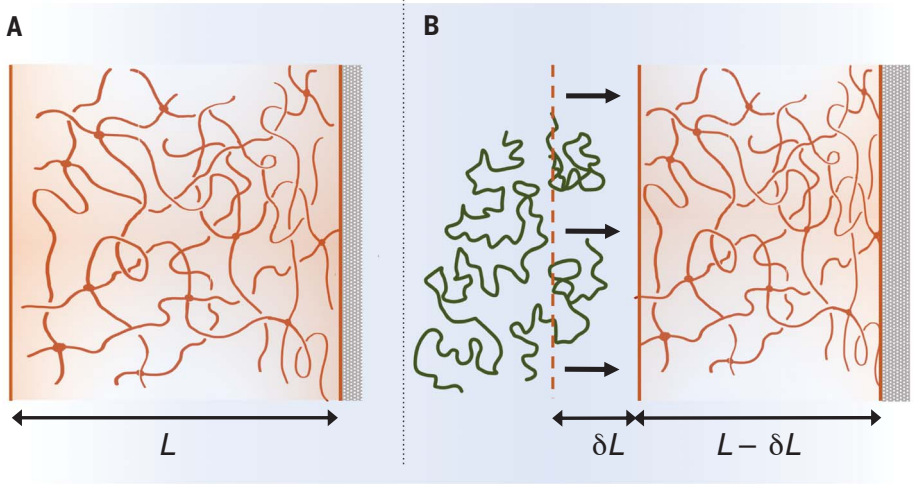

Fig. 3. Hydrogel deswelling. (**A**) A gel initially swollen to thickness L in pure solvent (**B**) de-swells by δL when an osmolyte lowers the osmotic pressure by $\delta\pi$.

Tanaka and co-workers verified Eq. 8 experimentally, using dynamic light scattering to measure D within swollen gels, macroscopic permeation measurements to determine ξ, mechanical experiments to measure elastic moduli (K and G, and therefore M), and swelling experiments to measure ϕ_s (*28*).

The second key relation connects the mechanical response properties (moduli) of the matrix to the equilibrium thermodynamics of swollen membranes (see the SM). Figure 3A shows a gel initially swollen to thickness L in pure solvent, which deswells when an osmolyte (e.g., a polymer excluded from the swollen gel) reduces the solvent activity a_s outside the membrane (Fig. 3B). The osmotic pressure difference exerts a stress $\delta\pi$ on the membrane, compressing the matrix until it is balanced by the elastic stress $-M\nabla\cdot u$. Solving this stress balance gives the longitudinal osmotic modulus M

$$M = \frac{RT}{\overline{V}_s}\frac{\phi_p^0}{\phi_s^0}\left.\frac{\partial\ln a_s}{\partial\ln\phi_s}\right|_{T;\phi_s^0} \quad (9)$$

in terms of the thermodynamic relation between solvent swelling (ϕ_s) and solvent activity (a_s).

Even without explicitly solving the FS equations (Eqs. 4 to 6), Eqs. 8 and 9 reveal three distinct expressions for the permeability

$$\kappa_{SD} = \frac{D}{1-\phi_s}\left(\frac{\phi_s\overline{V}_s}{RT}\left.\frac{\partial\ln\phi_s}{\partial\ln a_s}\right|_{T;\phi_s^0}\right) = \frac{D}{M} = \frac{\phi_s}{\xi} = \kappa_{PF} \quad (10)$$

to be quantitatively identical and to all follow from the FS model. The equality between the first two relates the thermodynamic factor in the general solution-diffusive flux (Eq. 3) to the compressional stiffness of the matrix using Eq. 9. The second equality relates the binary diffusivity to the mechanical membrane properties M and ξ (Eq. 8) to reproduce the PF permeability (Eq. 1). Although these permeability expressions appear very different, they simply reflect different ways of expressing the same, fundamental driving force—in purely thermodynamic terms (Eq. 3), in purely mechanical terms (Eq. 1), or in hybrid terms (Eq. 10).

Figure 4 shows FS model predictions (solutions to Eqs. 4 to 6) for a swollen membrane of equilibrium thickness L, through which a transmembrane pressure drop Δp drives a solvent flux J_s that is gentle enough to maintain a linear pressure-flux relationship. The polymer displacement u_p is highest $[L\Delta p/(2M)]$ on the upstream side and vanishes at the rigid support on the permeate side. The corresponding solvent concentration profile ϕ_s decreases linearly by $(1-\phi_s^0)\Delta p/M$ over the membrane thickness L, consistent with SD. Equal and opposite

gradients in ϕ_p, not shown, are required by space filling. The fluid-phase pressure p decreases continuously within the membrane, with constant gradient $-\Delta p/L$, while the compressive normal stress σ_p^{xx} on the polymer phase grows linearly from zero on the (uncompressed) feed side, to a maximum at the permeate side, with gradient equal and opposite to the fluid pressure.

Resolving discrepancies

The normal stress profiles in Fig. 4 clarify the different pressure profiles predicted by PF and SD—the key distinction ultimately reflects differences in how the two models define pressure. PF focuses exclusively on the mechanics of the solvent phase and uses p to refer to the hydrodynamic pressure within the solvent phase. SD, by contrast, combines solvent and polymer as one composite phase and uses p to mean the composite stress $\sigma_T = \sigma_s + \sigma_p$ of both fluid and solid components. Given that no other forces are exerted within the membrane, mechanical equilibrium requires σ_T to be constant—indeed, adding the polymer and solvent momentum equations (Eqs. 5 and 6) gives

$$\frac{\partial \sigma_T}{\partial x} = \frac{\partial \sigma_s}{\partial x} + \frac{\partial \sigma_p}{\partial x} = \xi v_s - \xi v_s = 0 \qquad (11)$$

Equation 11 holds irrespective of the specific form of the constitutive relations σ_s and σ_p or the solvent-polymer friction ξ. Treating the solvent and polymer phases separately, as in FS, gives a nonzero solvent-phase pressure gradient that is balanced by the elastic stress of the compressed network.

The FS profiles in Fig. 4 resolve the apparent discrepancies between PF and SD predictions of concentration and pressure fields. In particular, nonzero gradients arise for both concentration ϕ_s and fluid pressure p. Concentration gradients are required by SD but are assumed not to exist in PF. Likewise, the pressure gradient is required by PF but assumed to be zero in SD. In this regard, SD and PF are both correct in treating their respective gradient but incorrect in assuming the other gradient to be zero. Notably, the PF model does not require ϕ_s to be constant; it simply does not rely on a nonzero $\nabla\phi_s$. Similarly, no pressure gradient is needed to drive a SD flux; instead, mechanical equilibrium requires a constant normal stress.

Three small quantities arise in the linear-response limit of solvent permeation of a swollen gel: the solvent flux J_s, the solvent pressure gradient ∇p, and the solvent (or polymer) concentration gradient $\nabla\phi_s$. Each quantity is proportional to one of the others while neglecting the third. Solving the solvent equation alone relates J_s to ∇p, while ignoring $\nabla\phi_s$, giving the PF flux (Eq. 1). Enforcing polymer momentum alone relates J_s to $\nabla\phi_s$ and ignores ∇p; using Eq. 8 to eliminate M and ξ reproduces the general SD flux (Eq. 2). Finally, combining the fluid and solid momentum equations relates $\nabla\phi_p$ directly to ∇p, without explicit reference to J_s.

Consequences

In addition to bridging the two distinct models, the FS model brings qualitative and quantitative insight to experimental results that affect the research workflows in next-generation membranes. Recently, for example, the structural and dynamic properties of dry and swollen PARO membranes were studied using neutron scattering, with the explicit goal of identifying whether SD or PF correctly treated water permeation (*17*). Small-angle neutron scattering (SANS) found structural length scales to not change appreciably when swelling, and quasi-elastic neutron scattering (QENS) suggested water diffusivity $D \sim 2 \times 10^{-9}$ m^2/s, comparable to its self-diffusivity in bulk. Both results seemed inconsistent with SD, which requires coupled solvent/matrix diffusion driven by concentration gradients. Moreover, recent advances in microscopy revealed nanoscale density variations in PARO membranes (*36*), which could violate the homogeneity assumed by SD. These results motivated an argument that future PARO membranes should be developed to reduce tortuosity—as appropriate for PF—rather than working to enhance selective solubility.

Reassessing these results using the FS model, however, reveals no inconsistency. Namely, Eq. 8 connects the collective diffusivity D to hydraulic permeability κ through the longitudinal osmotic modulus M_0, which can be measured independently, for example, using a swelling pressure apparatus (*22*) or nanoindentation (*37*, *38*). Shin *et al.* measured both hydraulic permeance $P_w \sim 1.6$ liters per m^2·hour·bar and reduced Young's moduli ($E_r \sim 1.6$ GPa) of water-swollen PA membranes of thickness $L \sim 330 \pm 75$ nm (*38*). Using these measurements as characteristic of PARO films, the FS model predicts diffusivities $D = MP_wL \sim 2 \times 10^{-9}$ to 4×10^{-9} m^2/s. While the relatively large experimental uncertainties may be responsible for the aphysically high end of this range, the diffusivities measured by QENS has the magnitude expected for a membrane this stiff, with quantitative values consistent with FS predictions. Moreover, Shin *et al.* conditioned PARO membranes with a series of solvents, finding higher permeance P_w with softer moduli, as expected from Eq. 8, owing to the higher volume fraction ϕ_s and larger pore sizes (lower ξ) (*38*).

The FS model highlights the fundamentally interrelated nature of the mechanical (hydrodynamic) and thermodynamic (diffusive) mechanisms of solvent transport in osmotically active membranes. Collective diffusivity in PARO membranes is high because the swollen membrane is very stiff, owing to its high cross-link diffusivity, low swelling ratio, and therefore large thermodynamic factor. High cross-link densities give small mesh spacing (akin to pore size R_p), increasing the friction factor ξ and decreasing permeability κ.

Any case in which the FS connection fails to be made directly signals a breakdown in the universality of the mechanism governing solvent transport in the membrane. For example, dense polymer membranes for gas separation do not swell appreciably with added gas; rather, gas molecules dissolve into the free volume of the polymer network. Moreover, the pressure-driven flow of bulk gasses looks nothing like the molecular hopping of dissolved gas molecules. The elastic moduli of such membranes reflect

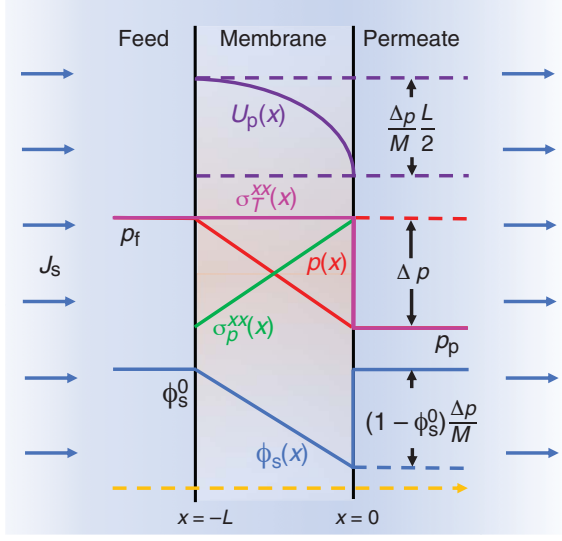

Fig. 4. Steady-state FS profiles across a solvent-swollen nonporous membrane bound to a permeable support at the permeate boundary. Polymer network displacement, purple (SM, eq. S73); normal solvent stress, red (eq. S63); normal polymer stress, green (eq. S75); normal composite stress, pink (Eq. 11); and solvent volume fraction, blue (eq. S76). A constant solvent flux J_s compresses the polymer network. Compression of the polymer network is dictated by the imposed pressure drop Δp and the modulus of uniaxial compression M. The sum of the solvent and polymer stress, that is, the normal composite stress, is constant throughout the membrane, with a discontinuity at the permeate boundary.

the compressibility of the polymer itself, with negligible influence of the gas phase. Likewise, the moduli of rigid, phase-separated, porous membranes (e.g., zeolites, macroporous polymers, or track-etched membranes) are not set by balancing the elastic stresses of the network against the mixing and solvating stresses of the solvent but instead reflect the stiffness of its elements and the morphology of the network. In both cases, the osmotic (free-draining) moduli of the networks are little affected by the presence (or absence) of solvent, breaking the interrelation between hydraulic and diffusive transport captured by the FS model. Whether the nanoscale heterogeneities observed in PARO membranes (*36*) violate the homogeneity assumed by SD and FS depends on whether they are osmotically active when hydrated and can therefore be treated as a swellable elastic network that is statistically homogeneous on length scales that are larger than the heterogeneities but smaller than membrane dimensions.

Another process involves high-pressure membrane performance under extreme pressures, as found in organic solvent nanofiltration (OSN) (*4*, *5*) and high-pressure reverse osmosis, for example, as is used for brine treatment (*39*–*41*). In these and other cases, membrane permeance decreases at high pressures, which has been hypothesized to result from membrane compaction (*4*, *39*, *41*).

Our analysis thus far has focused on lower-pressure permeation, where flux grows linearly with applied pressure. In this linear-response limit, the physical properties of the membrane change very little and are well approximated by their equilibrium values. Because the local friction coefficient ξ, longitudinal osmotic modulus M, and solvent velocity $v_s = j_s/\phi_s$ all depend on ϕ_s, concentration gradients can affect the flux expressions beyond their linear-response forms (Eq. 10).

The FS model provides a natural framework to understand, analyze, and predict nonlinear pressure-flux relations that are expected to arise in high-pressure reverse osmosis brine treatment (*39*–*41*) and OSN (*4*, *5*). Namely, the permeation flux stops increasing linearly at sufficiently high pressures, asymptotically approaching a limiting flux, as identified experimentally by Paul and Ebra-Lima (*5*) and in the OSN context (*4*). Hints of a limiting flux already appear in the leading-order FS solutions (Fig. 4), because $u_p \to L$ once $\Delta p \sim M$. The weak compression limit $\left(\delta\phi_p \ll \phi_p^0\right)$ is therefore only valid when Δp is much smaller than the longitudinal osmotic modulus M, which emerges as a natural scale for the transmembrane pressure. When $\Delta p \ll M$, polymer and solvent concentrations are perturbed only slightly, and the solvent flux varies linearly with Δp. When Δp approaches or exceeds M, however, the network compresses more substantially, the flux develops a nonlinear dependence on Δp, and material properties (e.g., M, ξ, ϕ_p, ϕ_s, and D) deviate substantially from their equilibrium values. A systematic perturbation solution to the unidirectional permeation problem, described in the SM, reveals the general first correction to the flux relation to be

$$J_s = \frac{\frac{D\Delta p}{M_0 L}}{1 + \frac{\Delta p}{2M_0}\left[-\phi_p^0(\ln\xi_0)' + \frac{\phi_p^0}{\phi_s^0} - 1\right]} \qquad (12)$$

where $(\ln\xi_0)' = d\ln\xi/d\phi_s\big|_{\phi_s^0} < 0$ captures the decrease in friction with solvent swelling. The second term in brackets reflects changes in flow velocity due to increased (compressed) polymer fraction ϕ_p, and the third reflects the decreased thickness of the compressed membrane.

The FS limiting flux relation (Eq. 12) justifies the empirical expression $a\Delta p/(1 + b\Delta p)$ found by Paul and Ebra-Lima to fit nonlinear flux measurements (*5*). Additionally, Eq. 12 predicts the physical form of the fitting parameters a and b and thus provides design guidance for future membranes. A key feature is that the longitudinal osmotic modulus M_0 sets the pressure scale above which the permeation flux starts to saturate. Although M_0 was not measured alongside the flux measurements, FS predicts the limiting (ceiling) flux at large pressure

$$J_s^{\text{ceiling}} \sim \frac{2D}{L}\left[-\phi_p^0(\ln\xi_0)' + \frac{\phi_p^0}{\phi_s^0} - 1\right]^{-1} \qquad (13)$$

to be independent of M_0, which can be compared to the measured ratio a/b. Paul and Ebra-Lima tabulated a, b, D, L, ϕ_p, and ϕ_s for 12 organic solvents in cross-linked rubber membranes (*5*); only $(\ln\xi_0)'$ was not determined. Basing ξ on Zick and Homsy's calculation of fluid flow through periodic arrays of rigid spheres (*19*) reveals Eq. 13 to predict measurements to within a factor of four for all 12 solvents (SM).

Furthermore, the fluid-solid model lays out a path to treat membranes for which neither the PF nor the SD approach is appropriate. For example, hydrogel pore-filled composite membranes (*42*) immobilize a homogeneous, nonporous polymer matrix within the pores of a rigid membrane support. The rigid pore walls constrain the deformations of the nonporous gel in a way that would be difficult to capture with SD, yet straightforward with FS. More generally, the FS approach provides a natural framework to treat mechanically heterogeneous membranes with rigid structural elements that pin or restrict the deformation of nonporous networks. Double network hydrogels (*43*, *44*), composed of an expanded rigid polymer mesh interpenetrated by an elastic swollen polymer network, have both high water content and high mechanical strength and toughness. Combining these two networks provides orthogonal control over permeability and mechanical stiffness and thus greater control over the limiting flux.

The FS model is primed to determine the dynamics of solutes and solvents in hydrogel systems placed under mechanical stresses or pressures—for example, hydrogels injected into the human body for drug delivery (*45*, *46*), tissue scaffolds (*47*), and chemomechanic sensors (*48*, *49*). The FS description of these bioengineered hydrogels connects system performance with material chemistry. Although we have specifically focused on binary solvent-polymer systems here, it is natural to expand the FS formulation to account for additional solute or solvent concentration fields, which occur both in membranes and more generally.

More broadly, the FS model lays out a framework for the design of membrane materials on the basis of ex situ characterizations. The degree of swelling $\left(\phi_s^0\right)$ and mechanical moduli (G, K, and M) may be measured macroscopically for a swollen gel of interest, and the collective diffusivity may be measured using dynamic light scattering, following Tanaka *et al.* (*28*), to give all the needed parameters for FS description. Moreover, performing such experiments while varying the osmotic pressure of the swelling solution could elucidate the dependence of M, ξ, and ϕ_s on osmotic or transmembrane pressure, providing a complete set of parameters for nonlinear flux relations such as Eq. 12. Finally, measuring these parameters as functions of the composition of the swelling solution (solvent mixtures, solute concentrations) would provide the parameters needed to predict multicomponent transport through membranes.

Here, we have shown that the pore-flow and solution-diffusion approaches both provide correct and consistent descriptions of solvent transport through nonporous, swollen membranes, despite the apparent discrepancies in their predictions of pressure and concentration profiles. These two approaches represent complementary descriptions of the same process and ultimately yield identical predictions. Neither approach is incorrect; instead, the predictions of one model are in perfect quantitative agreement with those of the other. After all, momentum and mass must both be conserved, mechanical and thermodynamic balances must both be respected. A subtle distinction between the two approaches lies in the phases they treat: Pore flow focuses exclusively on the liquid phase, whereas solution diffusion treats the polymer and solvent as a single, inseparable continuum phase. The fluid-solid model is general enough to enable transport modeling for membrane materials that neither of the classical models can handle. Given the central role of the longitudinal osmotic modulus M_0

in the fluid-solid model, it is imperative that it be measured as part of the standard suite of characterization experiments for swollen membranes (*50*).

REFERENCES AND NOTES

1. G. M. Geise *et al.*, *J. Polym. Sci. B Polym. Phys.* **48**, 1685–1718 (2010).
2. G. M. Geise, D. R. Paul, B. D. Freeman, *Prog. Polym. Sci.* **39**, 1–42 (2014).
3. J. G. Wijmans, R. W. Baker, *J. Membr. Sci.* **107**, 1–21 (1995).
4. H. Y. Jang *et al.*, *AIChE J.* **65**, e16757 (2019).
5. D. R. Paul, O. M. Ebra-Lima, *J. Appl. Polym. Sci.* **14**, 2201–2224 (1970).
6. L. F. Greenlee, D. F. Lawler, B. D. Freeman, B. Marrot, P. Moulin, *Water Res.* **43**, 2317–2348 (2009).
7. D. R. Paul, *J. Polym. Sci. Polym. Phys. Ed.* **11**, 289–296 (1973).
8. D. R. Paul, *J. Polym. Sci. Polym. Phys. Ed.* **12**, 1221–1230 (1974).
9. D. R. Paul, *Separ. Purif. Methods* **5**, 33–50 (1976).
10. M. L. White, *J. Phys. Chem.* **64**, 1563–1565 (1960).
11. H. Yasuda, C. E. Lamaze, A. Peterlin, *J. Polym. Sci. A-2 Polym. Phys.* **9**, 1117–1131 (1971).
12. A. Peterlin, H. Yasuda, *J. Polym. Sci. Polym. Phys. Ed.* **12**, 1215–1220 (1974).
13. M. Qasim, M. Badrelzaman, N. N. Darwish, N. A. Darwish, N. Hilal, *Desalination* **459**, 59–104 (2019).
14. P. M. Biesheuvel, S. Porada, M. Elimelech, J. E. Dykstra, *J. Membr. Sci.* **647**, 120221 (2022).
15. L. Song, M. Heiranian, M. Elimelech, *Desalination* **520**, 115360 (2021).
16. W. K. Kim, S. Milster, R. Roa, M. Kanduč, J. Dzubiella, *Macromolecules* 10.1021/acs.macromol.2c00605 (2022).
17. E. P. Chan *et al.*, *Macromolecules* **53**, 1443–1450 (2020).
18. E. M. Furst, T. M. Squires, *Microrheology* (Oxford Univ. Press, 2018).
19. A. A. Zick, G. M. Homsy, *J. Fluid Mech.* **115**, 13–26 (1982).
20. S. Rosenbaum, O. Cotton, *J. Polym. Sci. A-1 Polym. Chem.* **7**, 101–109 (1969).
21. J. S. Ham, M. C. Bolen, J. K. Hughes, *J. Polym. Sci.* **57**, 25–40 (1962).
22. S. D. Gehman, *Rubber Chem. Technol.* **40**, 532–543 (1967).
23. M. A. Biot, *J. Appl. Phys.* **12**, 155–164 (1941).
24. M. A. Biot, *J. Appl. Mech.* **23**, 91–96 (1956).
25. M. A. Biot, D. G. Willis, *J. Appl. Mech.* **24**, 594–601 (1957).
26. M. Tokita, T. Tanaka, *J. Chem. Phys.* **95**, 4613–4619 (1991).
27. T. Tanaka, D. J. Fillmore, *J. Chem. Phys.* **70**, 1214–1218 (1979).
28. T. Tanaka, L. O. Hocker, G. B. Benedek, *J. Chem. Phys.* **59**, 5151–5159 (1973).
29. M. Doi, *J. Phys. Soc. Jpn.* **78**, 052001 (2009).
30. C. Y. Hui, V. Muralidharan, *J. Chem. Phys.* **123**, 154905 (2005).
31. J. Yoon, S. C. Cai, Z. Suo, R. C. Hayward, *Soft Matter* **6**, 6004–6012 (2010).
32. D. Chen, J. Yoon, D. Chandra, A. J. Crosby, R. C. Hayward, *J. Polym. Sci. B Polym. Phys.* **52**, 1441–1461 (2014).
33. R. B. Bird, W. E. Stewart, E. N. Lightfoot, *Transport Phenomena, Revised 2nd Edition* (John Wiley & Sons, 2006).
34. L. D. Landau, E. M. Lifshitz, *Theory of Elasticity*, vol. 7 of *Course of Theoretical Physics*, J. B. Sykes, W. H. Reid, Trans. (Addison-Wesley, 1959).
35. T. Tanaka, S. Ishiwata, C. Ishimoto, *Phys. Rev. Lett.* **38**, 771–774 (1977).
36. T. E. Culp *et al.*, *Science* **371**, 72–75 (2021).
37. Y. Hu, X. Zhao, J. J. Vlassak, Z. Suo, *Appl. Phys. Lett.* **96**, 121904 (2010).
38. M. G. Shin *et al.*, *J. Membr. Sci.* **578**, 220–229 (2019).
39. M. T. M. Pendergast, J. M. Nygaard, A. K. Ghosh, E. M. Hoek, *Desalination* **261**, 255–263 (2010).
40. D. M. Davenport *et al.*, *J. Membr. Sci.* **610**, 118268 (2020).
41. D. M. Davenport, A. Deshmukh, J. R. Werber, M. Elimelech, *Environ. Sci. Technol. Lett.* **5**, 467–475 (2018).
42. N. Adrus, M. Ulbricht, *J. Mater. Chem.* **22**, 3088–3098 (2012).
43. J. P. Gong, *Soft Matter* **6**, 2583–2590 (2010).
44. S. Ahmed, T. Nakajima, T. Kurokawa, M. Anamul Haque, J. P. Gong, *Polymer* **55**, 914–923 (2014).
45. T. R. Hoare, D. S. Kohane, *Polymer* **49**, 1993–2007 (2008).
46. J. Li, D. J. Mooney, *Nat. Rev. Mater.* **1**, 16071 (2016).
47. J. M. Cloyd *et al.*, *Eur. Spine J.* **16**, 1892–1898 (2007).
48. H. Ding *et al.*, *Carbohydr. Polym.* **248**, 116797 (2020).
49. G. Lin, S. Chang, C. H. Kuo, J. Magda, F. Solzbacher, *Sens. Actuators B Chem.* **136**, 186–195 (2009).
50. J. M. Dennison, X. Xie, C. J. Murphy, D. G. Cahill, *ACS Appl. Nano Mater.* **1**, 5008–5018 (2018).

ACKNOWLEDGMENTS

Funding: This work was supported as part of the Center for Materials for Water and Energy Systems (M-WET), an Energy Frontier Research Center funded by the US Department of Energy, Office of Science, Basic Energy Sciences under award DE-SC0019272. **Author contributions:** V.H.H.: Conceptualization, Formal analysis, Investigation, Methodology, Validation, Writing – original draft, and Writing – review & editing. M.F.D.: Conceptualization, Writing – review & editing, Supervision, Project administration, and Funding acquisition. T.M.S.: Conceptualization, Formal analysis, Investigation, Methodology, Validation, Writing – original draft, Writing – review & editing, Supervision, Project administration, and Funding acquisition. **Competing interests:** None declared. **Data and materials availability:** All data needed to evaluate the conclusions in the paper are present in the paper or the supplementary materials.

SUPPLEMENTARY MATERIALS

science.org/doi/10.1126/science.abm7192
Supplementary Text
Table S1
Nomenclature
References

Submitted 6 October 2021; accepted 17 May 2022
10.1126/science.abm7192